Interbasin and interhemispheric impacts of a collapsed Atlantic Overturning Circulation

Bryam Orihuela-Pinto [1,2], Matthew H. England [1,3] ✉ and Andréa S. Taschetto [1,2]

Climate projections suggest a weakening or collapse of the Atlantic Meridional Overturning Circulation (AMOC) under global warming, with evidence that a slowdown is already underway. This could have significant ramifications for Atlantic Ocean heat transport, Arctic sea ice extent and regional North Atlantic climate. However, the potential for far-reaching effects, such as teleconnections to adjacent basins and into the Southern Hemisphere, remains unclear. Here, using a global climate model we show that AMOC collapse can accelerate the Pacific trade winds and Walker circulation by leaving an excess of heat in the tropical South Atlantic. This tropical warming drives anomalous atmospheric convection, resulting in enhanced subsidence over the east Pacific and a strengthened Walker circulation and trade winds. Further teleconnections include weakening of the Indian and South Atlantic subtropical highs and deepening of the Amundsen Sea Low. These findings have important implications for understanding the global climate response to ongoing greenhouse gas increases.

The Atlantic Meridional Overturning Circulation (AMOC) plays a fundamental role in Earth's climate via its control of poleward ocean heat transport[1]. The global climate state during an AMOC shutdown has been shown to be fundamentally different to when the AMOC is on, characterized by an expansion of Arctic sea ice, a colder Northern Hemisphere and a southward shift of the Intertropical Convergence Zone (ITCZ)[2–4]. This has occurred in the past and has been linked to past abrupt climate change[5–7]. At present, there is evidence that the AMOC is declining during the modern climate record[8–11] and, furthermore, it is projected to slowdown and potentially even collapse under anthropogenic global warming[12].

The AMOC stability relies on an intricate balance of temperature and salinity which cause density changes making it a nonlinear system with multiple stable states[13]. Even though a full AMOC collapse is not a high probability scenario, it is not a discarded possibility[14–16]. Furthermore, current models predicting its decline do not take into account the role of land ice melt[17], which would act to increase the likelihood of a shutdown via salinity changes[18]. This effect would be in addition to the temperature changes caused by anthropogenic global warming, which is the main driver of an AMOC slowdown in future projection models[19]. Given the nonlinearity and tipping point behaviour of the AMOC as well as its major impact on global climate, further research into its role in controlling the far-field ocean–atmosphere circulation is required.

The potential impact of an AMOC collapse goes beyond the Atlantic Ocean[2,3], with previous studies suggesting changes reaching the tropical Pacific. However, the way the tropical Pacific might respond to an AMOC collapse remains uncertain, with no consensus on how the trade winds and equatorial surface temperatures might change in response to an AMOC shutdown[4,20–22]. Addressing these discrepancies is crucial to understanding the effects of an AMOC collapse on global climate. In this study, we investigate the impact of an AMOC shutdown on global climate, including its effects on interbasin teleconnections to the tropical Pacific and Indian Oceans, as well as interhemispheric teleconnections to Antarctic climate.

We find that an AMOC collapse drives a complex rearrangement of the global atmospheric circulation that affects all latitudes, from the tropics to the polar circulation of both hemispheres. We find that changes in the tropical Pacific involve a robust intensification of the Walker circulation, a weakening of the subtropical highs in the Southern Hemisphere and an intensification of the Amundsen Sea Low over west Antarctica.

Model set-up and experimental design

The Community Earth System Model (CESM) v.1.2 global climate model is used to perform two sets of experiments (Methods); the first ensemble set is based on a pre-industrial control simulation (*AMOC-on*) wherein the AMOC exhibits a realistic modern-day overturning circulation (Fig. 1; Methods), while the second set is derived from runs perturbed by meltwater so that the AMOC collapses (*AMOC-off*). Note that the CESM model is particularly skilful in representing key climatic processes involved in this study, namely the AMOC[23], the Pacific mean state including the Walker circulation and coupled ocean–atmosphere feedbacks[24], and Atlantic–Pacific interbasin interactions (Methods; Extended Data Fig. 1). A total of five 100-yr ensemble members are generated for each experiment. All ensemble members were branched off different initial conditions 10 years apart using the equilibrated pre-industrial control *AMOC-on* experiment, with the only difference in set-up being the application of a freshwater flux to suppress the Atlantic overturning in the *AMOC-off* ensemble members. The strength of the AMOC in the *AMOC-off* experiments is weakened by ~20 Sv ($1\,Sv = 10^6\,m^3\,s^{-1}$), down to values of only ~3–4 Sv after year 50 (Fig. 1c); thereafter it remains at around this value for the rest of the simulation.

The main analyses shown in this study are derived from differences between the last 50 years of the *AMOC-off* case and the equivalent 50 years from the *AMOC-on* run. Similar analyses run over the last 20 of the experiments show robust results. In addition to analysing the equilibrated *AMOC-off* run relative to the *AMOC-on* control experiment, we also explore the transient adjustment of the

[1]Climate Change Research Centre, University of New South Wales, Sydney, New South Wales, Australia. [2]ARC Centre of Excellence for Climate Extremes, University of New South Wales, Sydney, New South Wales, Australia. [3]ARC Australian Centre for Excellence in Antarctic Science, University of New South Wales, Sydney, New South Wales, Australia. ✉e-mail: M.England@unsw.edu.au
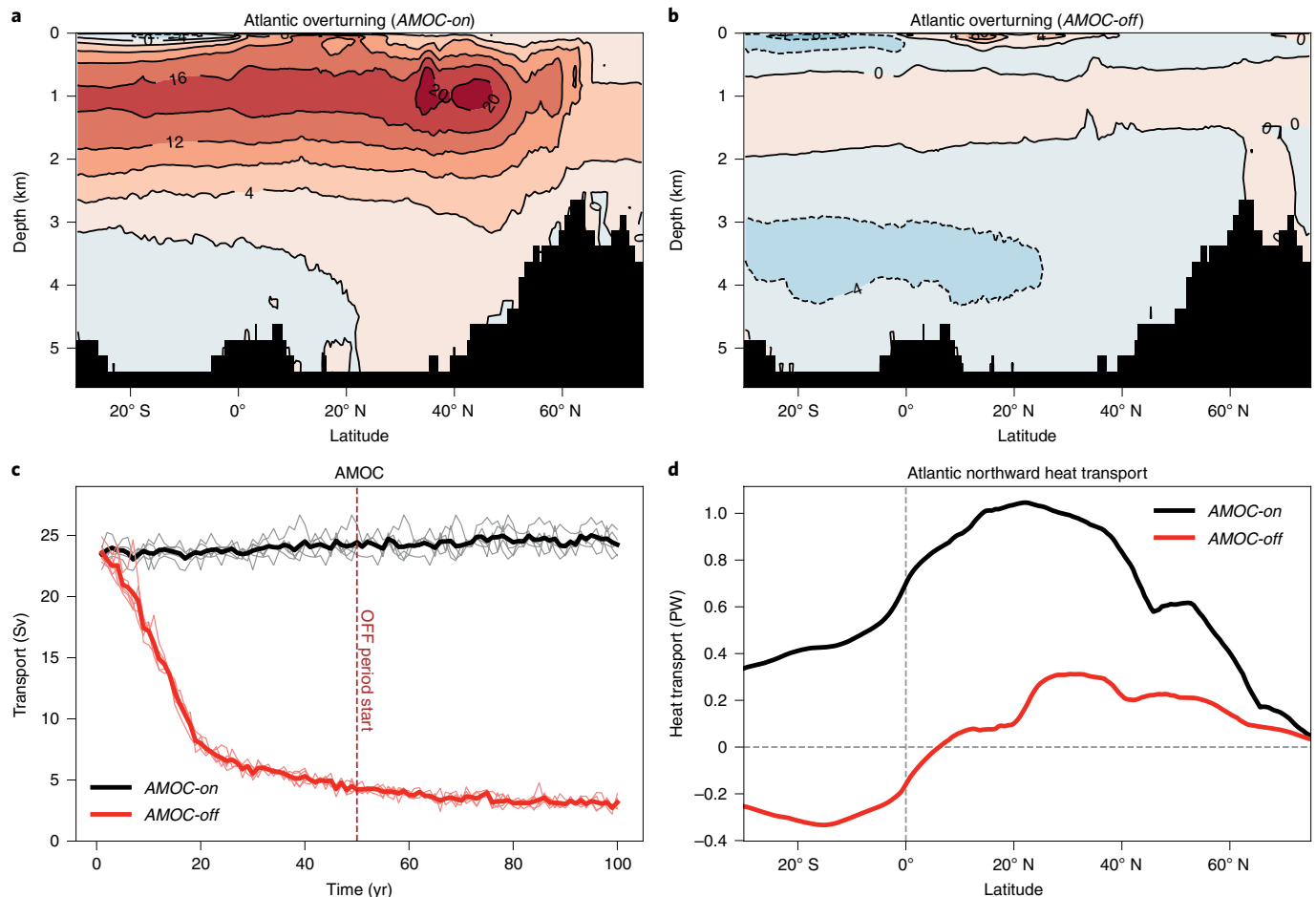
Fig. 1 | Meridional overturning and poleward heat transport in the model simulations. a,b, Mean meridional streamfunction (Sv; $1\,Sv = 10^6\,m^3\,s^{-1}$) in the Atlantic in *AMOC-on* (**a**) and *AMOC-off* (**b**) derived from the average of the last 50 years of the five member ensemble of simulations. **c,** Annual maximum of the AMOC streamfunction (Sv) in the *AMOC-on* and *AMOC-off* cases versus time, with individual ensemble members shown using thin lines and ensemble mean as bold lines. The maximum of the AMOC streamfunction is obtained between latitudes 25° N–75° N and between depths of 500 and 2,000 m for *AMOC-on* (black) and *AMOC-off* (red). **d,** Mean Atlantic Ocean northward heat transport (PW) in *AMOC-on* (black line) and *AMOC-off* (red line) over the last 50 years of the experiment.

coupled ocean–atmosphere system to AMOC collapse, by examining the development of decadal climatic anomalies subsequent to the initial freshwater perturbation.

Global surface ocean temperature response

As the maximum ocean heat transport in the North Atlantic (Fig. 1d) is greatly reduced with an AMOC collapse, a strong sea surface temperature (SST) cooling is established in the Northern Hemisphere oceans (Fig. 2a). The cooling anomalies initially appear in the North Atlantic high latitudes (Fig. 3a) along with a sea ice expansion, which in turn amplifies cooling in the area by reflecting incoming radiation back to space. The cooling gradually extends southwards reaching the northern mid-latitudes within the first 10 years of the *AMOC-off* simulation (Fig. 3a). From there, the cooling signal is progressively advected southward to the tropical Atlantic via the wind–evaporation–SST (WES) feedback[25,26]. Anomalous northeasterly winds that develop across the tropical North Atlantic (Fig. 4) enhance the evaporative cooling, reducing SST and expanding the cooling southward until it reaches the tropical North Atlantic by around year 20 (Fig. 3).

In the North Pacific high latitudes, cool SST anomalies appear by around year 5 and are well established by year 20 (Fig. 3a,b). The rapid onset of cooling in the North Pacific is probably due

to advection of the North Atlantic temperature anomalies via the mean westerly winds. On longer timescales, cooling could also happen via the Bering Strait throughflow[27]. The North Pacific cooling ultimately causes sea ice to expand in this ocean basin, which reinforces the cooling via the sea ice albedo feedback. A southward displacement of the cool anomalies into the tropical North Pacific can also be explained by the WES feedback, similar to the North Atlantic basin. However, as the AMOC slows down a synchronous cooling commences in the equatorial Pacific, maturing by around year 30 (Fig. 3 and Extended Data Fig. 2), evolving to La Niña-like conditions. This in turn weakens the Aleutian Low (Figs. 2c and 4), which is a teleconnection that is known to occur during La Niña events[28]. The equatorial Pacific cooling is associated with a strong intensification of the Pacific trade winds (Fig. 4 and Extended Data Fig. 2), which drive enhanced equatorial upwelling and westward advection of cool waters, as well as a spin up of the shallow tropical overturning cells.

With less northward ocean heat transport out of the South Atlantic (Fig. 1d), much of the Southern Hemisphere warms in response to the AMOC shutdown (Fig. 2a). This signal of hemispheric warming matures after around three decades (Fig. 3), contrasting the more rapid cooling of the northern oceans. The Southern Hemisphere warming is mainly a result of slower oceanic
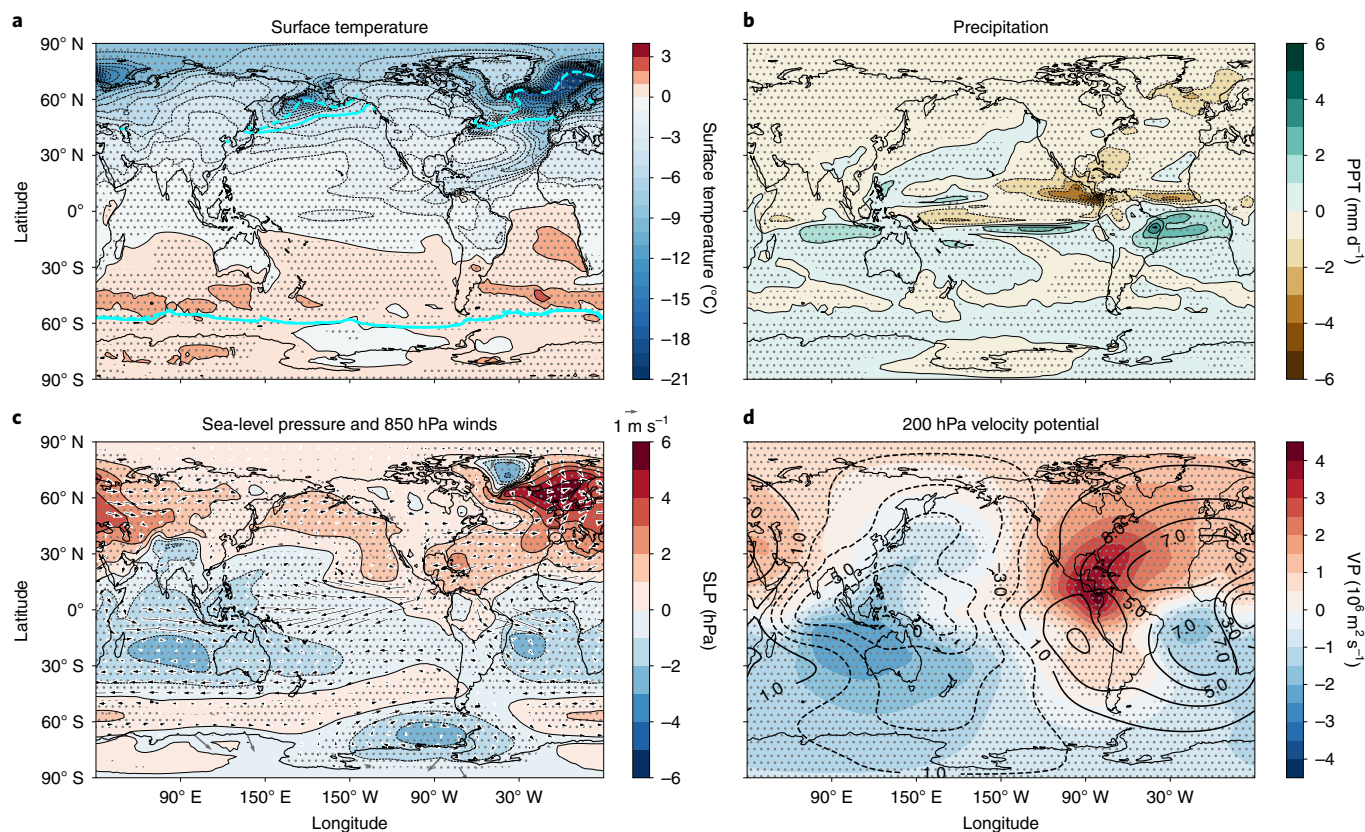
Fig. 2 | Response of the global climate system to AMOC shutdown. Shown as the difference between the ensemble mean of *AMOC-off* minus *AMOC-on*, annually averaged over years 51–100. **a**–**d**, Variables shown include surface temperature (°C; note the asymmetric colour scale) with contours of sea ice extent indicated for the *AMOC-on* (dashed) and *AMOC-off* (solid) runs in cyan (**a**), precipitation (PPT, mm d⁻¹) (**b**), sea-level pressure (SLP, hPa) colour-shaded with 850 hPa winds (m s⁻¹) overlaid as vectors (**c**) and velocity potential (VP) at 850 hPa (with contours indicated for *AMOC-on* mean) (**d**). The surface temperature in **a** is equivalent to SST over open ocean areas. Significant differences based on a Student's *t*-test at 95% significance level are hatched for shadings and bold for vectors.

adjustments associated with the reduction of oceanic heat transport out of the South Atlantic (Fig. 1d). In this way, the *AMOC-off* state ultimately features a widespread cooling over all the Northern Hemisphere and a modest warming across much of the south, creating an anomalous interhemispheric temperature gradient. This is consistent with previous model studies wherein the AMOC is shutdown[2–4]. However, our results also reveal a new feature that has not been previously discussed in the literature: namely, a marked intensification of the Walker circulation and widespread cooling along much of the equatorial Pacific.

Global atmospheric response
The weakening of the oceanic heat transport northward from the South Atlantic results in an anomalous northward atmospheric cross-equatorial heat flux to maintain the global energy balance. In other words, to compensate for the oceanic heat transport changes, the global atmospheric circulation is altered to increase heat transport from the warmer to the cooler hemisphere. The resulting circulation sees a strengthening of the Hadley cell in the Northern Hemisphere (Fig. 5a) and a displacement of the ITCZ toward the south (Fig. 2b). This relationship between cross-equatorial oceanic heat transport and ITCZ location agrees with previous work on the interplay between ocean and atmosphere energy fluxes[29]. It is the reorganization of the atmospheric circulation alongside SST changes that drives strong changes over the lower atmosphere.

Sea-level pressure intensifies over the northern high latitudes (Fig. 2c) where the coolest SST anomalies are located. At the northern

subtropical latitudes, there is an overall increase in pressure in response to the strengthened descending branch of the northern Hadley cell. Conversely, over the southern subtropics the weakened descending branch of the southern Hadley cell leads to a decrease in sea-level pressure. This suggests that the semipermanent highs are shifted equatorward and intensified in the Northern Hemisphere, while the opposite tendency occurs in the Southern Hemisphere. The weakening of the subtropical highs is particularly clear in the Indian Ocean and the South Atlantic (Fig. 2c), where an anomalous low pressure centre and cyclonic geostrophic wind anomalies develop. However, the South Pacific high shows a more modest response, since it is under the influence of the central Pacific cooling and an associated Rossby wave-train pattern across the basin. Wave-trains emanating from the tropics to high latitudes are a typical response to tropical Pacific cooling in both hemispheres[30]; the development of this response can be seen in the simulated difference fields of geopotential height in the upper troposphere (Extended Data Fig. 3). In fact, these wave-trains are what shapes the most significant response in the northern and southern high latitudes, ultimately resulting in a weakening of the Aleutian Low and a deepening of the Amundsen Sea Low (Fig. 2c).

The main effect of the AMOC collapse on precipitation is seen in the tropics, corresponding to the southward displacement of the ITCZ (Fig. 2b). There is an overall increase in precipitation along the southern portion of the ITCZ and reduced rainfall to the north. This becomes a clear feature after year 30 of the simulation (Extended Data Fig. 4). Before then, precipitation is reduced over
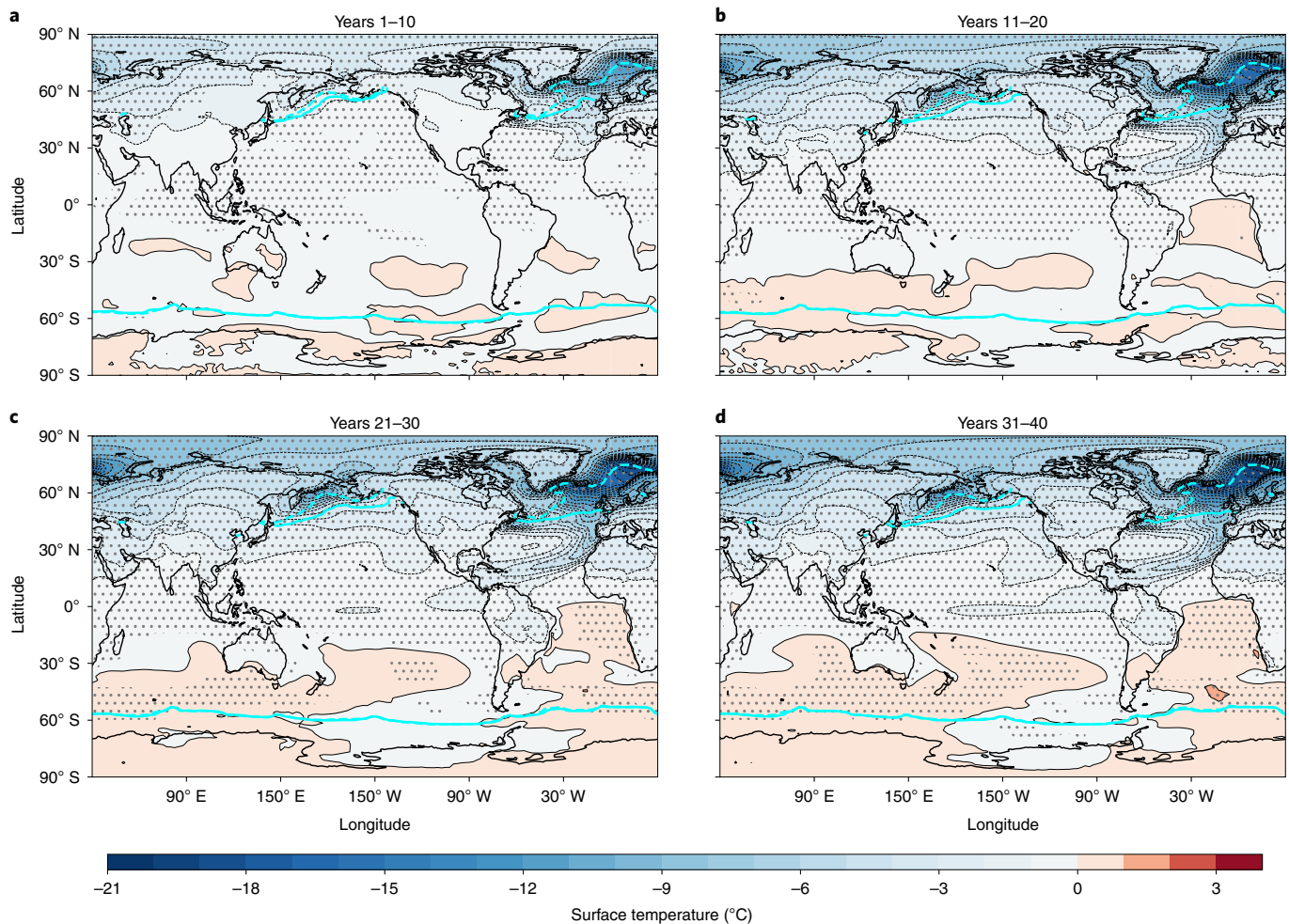
Fig. 3 | Transient response of surface temperature and sea ice to AMOC shutdown. Shown are the transient anomalies of decadal mean surface temperature (°C) and sea ice extent in response to a meltwater-induced AMOC shutdown (*AMOC-off* ensemble mean minus *AMOC-on* ensemble mean). **a–d**, Time periods, years 1–10 (**a**), years 11–20 (**b**), years 21–30 (**c**) and years 31–40 (**d**). Note the asymmetric colour scale about zero for surface temperature. Contours of sea ice extent are indicated for the *AMOC-on* (dashed) and *AMOC-off* (solid) experiments. Surface temperature corresponds to SST over the open ocean. Significant differences based on a Student's *t*-test at 95% significance level are hatched.

areas with the strongest cooling in the northern latitudes during the first few years of the experiment. The clear southward shift of the ITCZ in each ocean basin is established once cooling reaches the northern tropical latitudes and warming occurs just south of the Equator, highlighting the effect of the interhemispheric temperature gradient on precipitation anomalies. This is how the full pattern of precipitation change due to the AMOC shutdown (Fig. 2b) is obtained.

Surface winds in the southern extratropics adjust geostrophically to changes in atmospheric pressure, generating anomalous cyclonic circulation in response to the weakening of the subtropical highs in the Indian and South Atlantic Oceans and the strengthening of the Amundsen Sea Low (Fig. 2c). In the tropics, wind changes are consistent with the southward ITCZ shift, particularly in the Indian and Atlantic Oceans, where an anomalous cross-equatorial wind pattern is established; with westerly anomalies to the north and easterly anomalies to the south[31]. However, the Pacific response is more complex, involving local ocean–atmosphere feedbacks as well as interbasin teleconnections. Initially there is a trade wind acceleration in the east Pacific during years 11–20 (Fig. 4b) driven by the pressure gradient between the North Atlantic and Pacific Oceans across the Panama Isthmus[32]. In the decades that follow (Fig. 4c,d), the east Pacific trade wind acceleration extends

westward along the tropical Pacific, due to both enhanced tropical South Atlantic convection and local Bjerknes feedbacks, both of which act to accelerate the Pacific Walker cell (Extended Data Figs. 5c,d and 6b). This mechanism is explained in more detail in the following section.

Walker circulation changes
In addition to the meridional atmospheric circulation changes induced by the intensification of the northern Hadley cell, the zonal equatorial circulation also responds to the AMOC collapse. In particular, there is a strengthening of the Walker cells in all ocean basins (Fig. 5b). This strengthening is particularly strong in the Pacific, where enhanced subsidence leads to intensified low level easterly winds. The anomalous subsidence in the east Pacific is tightly related to enhanced deep convection over the Atlantic, where the strongest upward anomalies among all ocean basins occur.

In the transient response (Extended Data Fig. 5) the upward motion in the equatorial Atlantic starts by year 20, initially generating anomalous subsidence and easterlies localized over the eastern Pacific. However, by year 30 the upward motion in the equatorial Atlantic intensifies, and the subsidence over the Pacific sector is enhanced, extending to the central and western Pacific. The westward propagation of anomalous surface easterlies along with cool
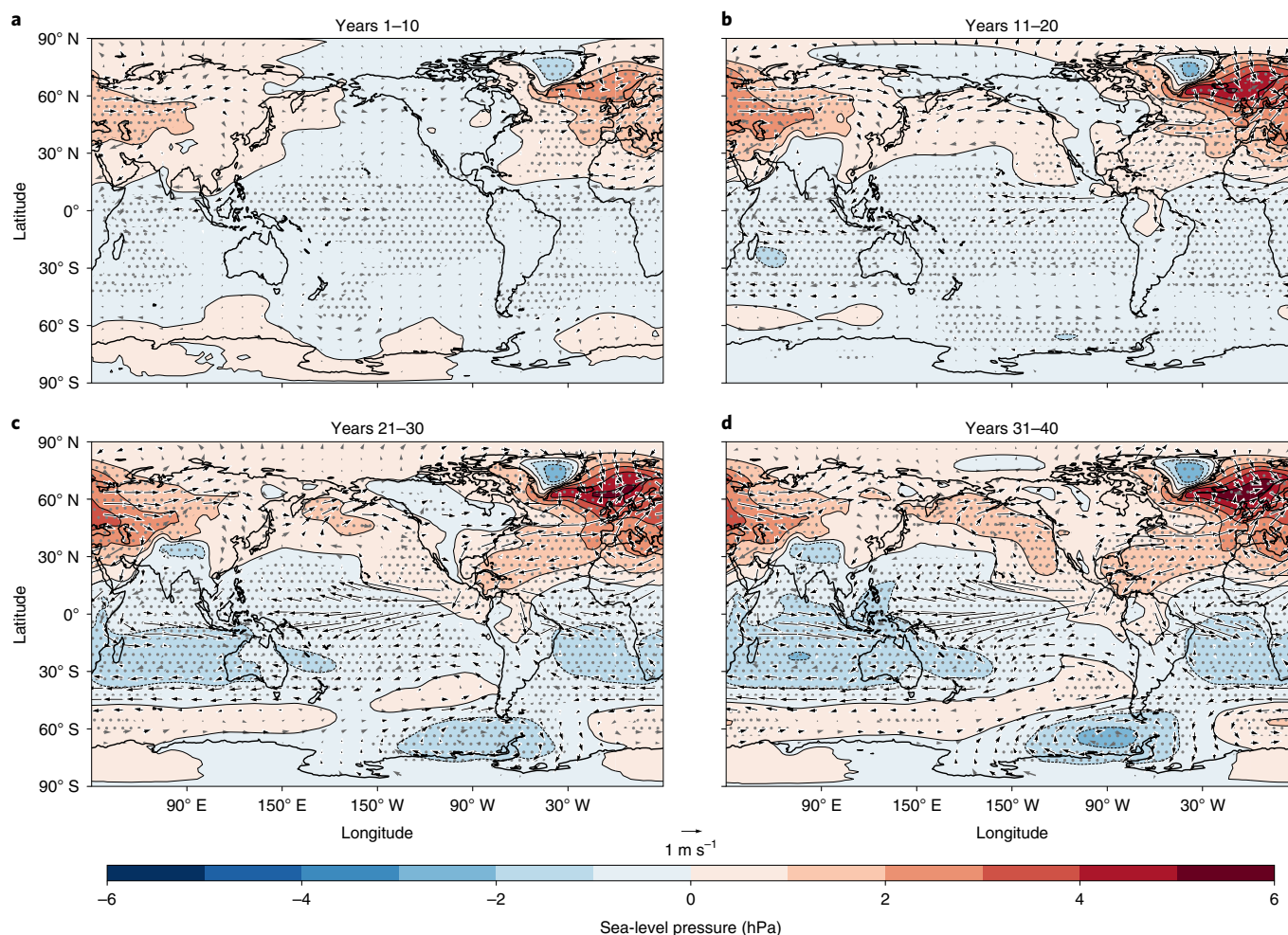
Fig. 4 | Transient response of sea-level pressure and near-surface winds to AMOC shutdown. Shown are the transient anomalies of sea-level pressure and near-surface winds in response to a meltwater-induced AMOC shutdown (*AMOC-off* ensemble mean minus *AMOC-on* ensemble mean). **a–d**, Time periods, years 1–10 (**a**), years 11–20 (**b**), years 21–30 (**c**) and years 31–40 (**d**). Each panel shows the decadal mean anomalies in sea-level pressure (hPa) colour-shaded, with 850 hPa wind differences (m s⁻¹) overlaid as vectors. Significant differences based on a Student's *t*-test at 95% significance level are hatched and made bold for vectors.

SST anomalies extending from the eastern Pacific is also enhanced by a local Bjerknes feedback. This westward propagation of cool surface water and easterly wind anomalies is typical during cold (La Niña) events in the Pacific[33,34].

The finding that tropical convection in the Atlantic is enhanced and drives the Pacific Walker circulation intensification in *AMOC-off* might at first seem counterintuitive, given that the tropical North Atlantic has cool SST anomalies and that past studies[35–37] found warming in this area to cause a similar effect. However, here, the origin of anomalous convection can be traced to the tropical South Atlantic, where relatively warm SST anomalies develop (Fig. 2a). In particular, these local warm SST anomalies drive anomalous convection (Fig. 2b) and upper-level divergence (Fig. 2d) in the tropical South Atlantic, consistent with the southward migration of the ITCZ (Fig. 2b). This can also be seen when the Walker circulation is separated into its components just north and south of the Equator (Extended Data Fig. 6), whereupon it becomes clear that most of the upward velocity anomalies occur just south of the Equator. Consequently, the anomalous tropical South Atlantic convection (Fig. 2b) drives enhanced subsidence (Fig. 5b) and upper-level convergence (Fig. 2d) over the east Pacific, accelerating the Pacific Walker circulation and hence cooling the tropical Pacific.

Discussion and summary

Our study investigates the potential climatic impacts and global atmospheric teleconnections of an AMOC shutdown. We find that an AMOC collapse drives a profound global-scale reorganization of the atmospheric circulation, initially triggered by a strong North Atlantic cooling and a southward migration of the ITCZ. In particular, we find that an AMOC shutdown drives a significant strengthening of the Pacific Walker circulation, something not previously described in the literature. The Walker circulation strengthening is triggered by enhanced low-level easterlies across the Panama Isthmus and reinforced by anomalous subsidence in the eastern Pacific from enhanced convection over the tropical South Atlantic. The stronger Pacific trade winds in turn lead to tropical central Pacific cooling and further Walker circulation acceleration. A positive Bjerknes feedback is established in a collapsed AMOC world, which forces the tropical Pacific into a more La Niña-like mean state.

The global-scale atmospheric and climatic changes driven by an AMOC collapse can be summarized in Fig. 6. These changes start with surface cooling over the North Atlantic and expanding Arctic sea ice, driven by reduced poleward heat transport in the Atlantic. The cooling then propagates into the North Pacific and
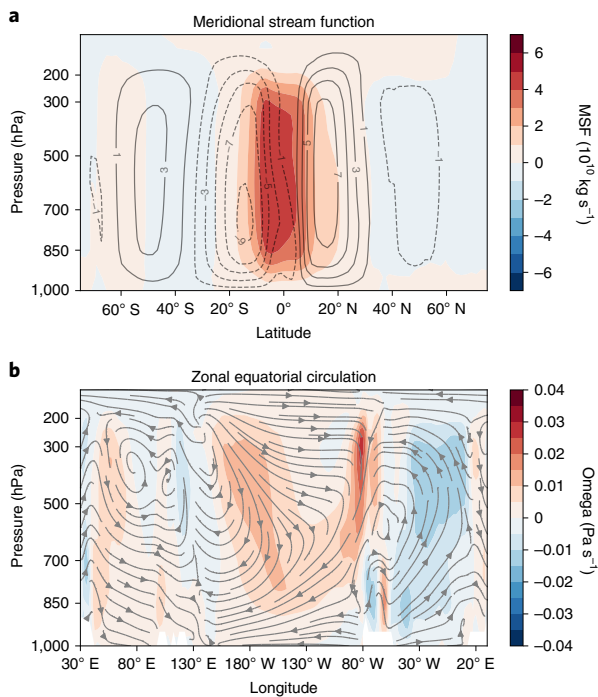
Fig. 5 | Large-scale atmosphere circulation response to AMOC shutdown.
a,b, Annual mean anomalies caused by the AMOC shutdown (shown as the ensemble average of *AMOC-off* minus *AMOC-on* for years 51–100) of zonally integrated atmospheric meridional streamfunction (shading; MSF, $10^{10}\,kg\,s^{-1}$) with control *AMOC-on* average circulation overlaid as contours ($10^{10}\,kg\,s^{-1}$) (**a**) and equatorial (5°S–5°N) mean atmospheric circulation (streamlines) and vertical velocity (shading; Omega, Pa s^{-1}) (**b**).

spreads southwards in both basins to reach the tropics. The reduction in oceanic heat transport also creates a net heat imbalance across the hemispheres, with excess heat remaining in the Southern Hemisphere and a deficit in the Northern Hemisphere. This generates an anomalous interhemispheric temperature gradient. The atmospheric circulation then compensates by intensifying and displacing the northern Hadley cell southward, which causes the ITCZ to also shift southward. The anomalous interhemispheric temperature gradient also impacts Atlantic–Pacific interbasin teleconnections. In particular, in the *AMOC-off* state, convergence in the upper troposphere and subsidence over the eastern equatorial Pacific are triggered by tropical South Atlantic warming. Hence, the intensified convection in the South Atlantic ultimately acts to enhance the Pacific Walker circulation and cool the tropical Pacific, which in turn causes interhemispheric teleconnections such as a deepening of the Amundsen Sea Low (Fig. 6).

These findings have implications for both past climate states and also future climate change. In particular, climate change projections predict a weakening and potential collapse of the AMOC[15], even without including the effects of Greenland ice melt. Our results suggest that such a collapse would significantly alter the Pacific Ocean response to climate change, with the Walker circulation strengthening by 32% under an AMOC shutdown (Methods; Extended Data Fig. 7). Given that most climate models project a weakening of the Walker circulation under global warming[38,39], with a median reduction of 10% by 2100 under a high emission scenario (Methods; Extended Data Fig. 7), this teleconnection from the Atlantic would dampen and perhaps even reverse this projected Walker circulation trend. Furthermore, we find that an AMOC collapse strengthens the northern Hadley cell by ~8% in *AMOC-off* (Methods), which would counteract the projected weakening of the northern Hadley cell[39,40]. In the South Pacific sector of the Antarctic margin, an AMOC collapse would further contribute to projected Amundsen Sea Low
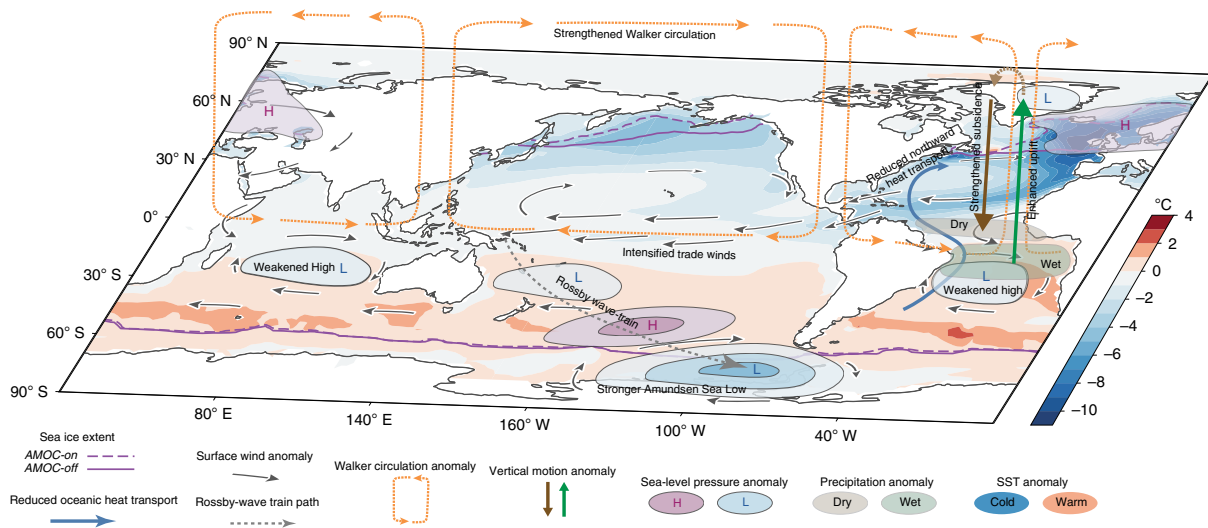

Fig. 6 | Schematic of the global climatic response to AMOC shutdown. Highlighted are the interbasin and interhemispheric changes in atmospheric circulation as well as the surface temperature difference (shading) between *AMOC-off* and *AMOC-on*. An AMOC shutdown reduces the oceanic heat transport in the Atlantic (blue arrow), leading to a cooling in the North Atlantic (blue shading) and sea ice expansion (dashed and solid purple lines). The atmospheric cooling is advected into the North Pacific and tropical North Atlantic via winds as well as a wind–evaporation–SST feedback, while anomalous heat remains in the Southern Hemisphere, creating an anomalous interhemispheric temperature gradient. This leads to a reorganization of the meridional atmosphere circulation, which weakens the subtropical highs in the Southern Hemisphere (light blue low pressure centres). The AMOC shutdown also displaces the ITCZ southward, leading to drier conditions (brown shading) in the tropical North Atlantic and wetter conditions (green shading) in the tropical South Atlantic. Warm SST anomalies in the South Atlantic favour enhanced convection (green upward arrow) that strengthens the local Walker circulation, driving anomalous subsidence in the equatorial east Pacific. The temperature difference and pressure gradient between the tropical North Atlantic and tropical Pacific generates anomalous winds that intensify the equatorial Pacific trade winds (grey arrows). The intensification of the Pacific trade winds strengthens the Walker circulation (orange dotted arrows) triggering the Bjerknes feedback that puts the tropical Pacific into a more La Niña-like state. The changes in the tropical Pacific mean state are conducive to a Rossby wave-train (grey dashed arrow) that leads to an intensification of the Amundsen Sea Low over west Antarctica.

changes[41], with this low pressure system deepening by ~2 hPa in *AMOC-off* (Methods). The AMOC teleconnection to the Pacific could also have further climatic impacts, such as setting the pace of decadal global temperature rise[42] or altering the nature and frequency of El Niño/Southern Oscillation (ENSO) events[43]. Our study has also demonstrated AMOC teleconnections to other remote locations, including the atmospheric circulation over the west Antarctic, with links to ice melt[44,45] and the strength of the subtropical highs in the Southern Hemisphere.

Regarding past climatic states, there is palaeoclimate evidence that during the Last Glacial Maximum the AMOC was shallower and weakened[46] along with a cooler central equatorial Pacific[47] and a stronger Walker circulation[48]. Our findings are consistent with this palaeo evidence, despite the differences in forcing and magnitude of the AMOC change. An AMOC weakening has also been associated with the Little Ice Age[49,50], an epoch that shares similar climate anomalies to the ones we describe here. In particular, there is evidence that during this time there was a southward migration of the ITCZ[51] and hydrological proxies suggest a westward shifted precipitation due to intensification of the Pacific Walker circulation[52], again consistent with our findings. Most recently, historical records since the mid-twentieth century suggest a long-term multidecadal weakening of the AMOC[9], coinciding with an overall intensification of both the Pacific Walker circulation[53] and the northern Hadley cell[54] and a deepening of the Amundsen Sea Low[55] (see Methods for recent trends).

The results presented here have been derived from a single model set-up under pre-industrial conditions, although, as discussed, the model used is particularly skilful in representing the main mechanistic features analysed in this study, namely the AMOC, the Pacific mean state and its variability and, importantly, Atlantic–Pacific interbasin interactions. Future work should examine how the impacts of an AMOC shutdown are further modulated under more complex scenarios, such as in past climate eras or in the future under a range of increasing greenhouse gas concentration scenarios. Nonetheless, the approach used here helps to isolate the effect of an AMOC shutdown from other factors and provides clues as to what teleconnections could play out in more complex scenarios. For future projections for example, where current climate models do not take into account the effects of ice sheet melt, there is an enhanced probability of an AMOC shutdown. In this case, the mechanisms described here would significantly alter the atmospheric response to global warming.

Online content

References

1. Buckley, M. W. & Marshall, J. Observations, inferences, and mechanisms of the Atlantic Meridional Overturning Circulation: a review. *Rev. Geophys.* **54**, 5–63 (2016).
2. Vellinga, M. & Wood, R. A. Global climatic impacts of a collapse of the Atlantic Thermohaline Circulation. *Clim. Change* **54**, 251–267 (2002).
3. Cheng, W., Bitz, C. M. & Chiang, J. C. H. in *Ocean Circulation: Mechanisms and Impacts—Past and Future Changes of Meridional Overturning* (eds Schmittner, A. et al.) 295–313 (American Geophysical Union, 2007).
4. Zhang, R. & Delworth, T. L. Simulated tropical response to a substantial weakening of the Atlantic Thermohaline Circulation. *J. Clim.* **18**, 1853–1860 (2005).
5. Clement, A. C. & Peterson, L. C. Mechanisms of abrupt climate change of the last glacial period. *Rev. Geophys.* **46**, RG4002 (2008).
6. Rahmstorf, S. Ocean circulation and climate during the past 120,000 years. *Nature* **419**, 207–214 (2002).
7. Clark, P. U., Pisias, N. G., Stocker, T. F. & Weaver, A. J. The role of the thermohaline circulation in abrupt climate change. *Nature* **415**, 863–869 (2002).
8. Rahmstorf, S. et al. Exceptional twentieth-century slowdown in Atlantic Ocean overturning circulation. *Nat. Clim. Change* **5**, 475–480 (2015).
9. Caesar, L., Rahmstorf, S., Robinson, A., Feulner, G. & Saba, V. Observed fingerprint of a weakening Atlantic Ocean overturning circulation. *Nature* **556**, 191–196 (2018).
10. Bryden, H. L., Longworth, H. R. & Cunningham, S. A. Slowing of the Atlantic meridional overturning circulation at 25° N. *Nature* **438**, 655–657 (2005).
11. Sun, C. et al. Atlantic Meridional Overturning Circulation reconstructions and instrumentally observed multidecadal climate variability: a comparison of indicators. *Int. J. Climatol.* **41**, 763–778 (2021).
12. Collins, M. et al. in *Climate Change 2013: The Physical Science Basis* (eds Stocker, T. F. et al.) 1029–1136 (Cambridge Univ. Press, 2013).
13. Manabe, S. & Stouffer, R. J. Two stable equilibria of a coupled ocean–atmosphere model. *J. Clim.* **1**, 841–866 (1988).
14. Bakker, P. et al. Fate of the Atlantic Meridional Overturning Circulation: strong decline under continued warming and Greenland melting. *Geophys. Res. Lett.* **43**, 252–12,260 (2016).
15. Liu, W., Xie, S.-P., Liu, Z. & Zhu, J. Overlooked possibility of a collapsed Atlantic Meridional Overturning Circulation in warming climate. *Sci. Adv.* **3**, e1601666 (2017).
16. Boers, N. Observation-based early-warning signals for a collapse of the Atlantic Meridional Overturning Circulation. *Nat. Clim. Change* **11**, 680–688 (2021).
17. Eyring, V. et al. Overview of the coupled model intercomparison project phase 6 (CMIP6) experimental design and organization. *Geosci. Model Dev.* **9**, 1937–1958 (2016).
18. Golledge, N. R. et al. Global environmental consequences of twenty-first-century ice-sheet melt. *Nature* **566**, 65–72 (2019).
19. Levang, S. J. & Schmitt, R. W. What causes the AMOC to weaken in CMIP5? *J. Clim.* **33**, 1535–1545 (2020).
20. Wu, L., Li, C., Yang, C. & Xie, S.-P. Global teleconnections in response to a shutdown of the Atlantic Meridional Overturning Circulation. *J. Clim.* **21**, 3002–3019 (2008).
21. Krebs, U. & Timmermann, A. Tropical air–sea interactions accelerate the recovery of the Atlantic Meridional Overturning Circulation after a major shutdown. *J. Clim.* **20**, 4940–4956 (2007).
22. Timmermann, A. et al. The influence of a weakening of the Atlantic Meridional Overturning Circulation on ENSO. *J. Clim.* **20**, 4899–4919 (2007).
23. Danabasoglu, G. et al. Variability of the Atlantic Meridional Overturning Circulation in CCSM4. *J. Clim.* **25**, 5153–5172 (2012).
24. Planton, Y. Y. et al. Evaluating climate models with the CLIVAR 2020 ENSO metrics package. *Bull. Am. Meteorol. Soc.* **102**, E193–E217 (2021).
25. Xie, S. P. A dynamic ocean–atmosphere model of the tropical Atlantic decadal variability. *J. Clim.* **12**, 64–70 (1999).
26. Chiang, J. C. H. & Bitz, C. M. Influence of high latitude ice cover on the marine Intertropical Convergence Zone. *Clim. Dynam.* **25**, 477–496 (2005).
27. Okumura, Y. M., Deser, C., Hu, A., Xie, S. P. & Timmermann, A. North Pacific climate response to freshwater forcing in the subarctic North Atlantic: oceanic and atmospheric pathways. *J. Clim.* **22**, 1424–1445 (2009).
28. Trenberth, K. E. et al. Progress during TOGA in understanding and modeling global teleconnections associated with tropical sea surface temperatures. *J. Geophys. Res. Ocean.* **103**, 14291–14324 (1998).
29. Schneider, T., Bischoff, T. & Haug, G. H. Migrations and dynamics of the intertropical convergence zone. *Nature* **513**, 45–53 (2014).
30. Hoskins, B. J. & Karoly, D. J. The steady linear response of a spherical atmosphere to thermal and orographic forcing. *J. Atmos. Sci.* **38**, 1179–1196 (1981).
31. McGee, D. et al. Hemispherically asymmetric trade wind changes as signatures of past ITCZ shifts. *Quat. Sci. Rev.* **180**, 214–228 (2018).
32. Xie, S. P., Okumura, Y., Miyama, T. & Timmermann, A. Influences of Atlantic climate change on the tropical Pacific via the Central American Isthmus. *J. Clim.* **21**, 3914–3928 (2008).
33. McPhaden, M. J. & Zhang, X. Asymmetry in zonal phase propagation of ENSO sea surface temperature anomalies. *Geophys. Res. Lett.* **36**, L13703 (2009).
34. Kang, I. S. & Kug, J. S. El Niño and La Niña sea surface temperature anomalies: a symmetry characteristics associated with their wind stress anomalies. *J. Geophys. Res. Atmos* **107**, 372 (2002).
35. McGregor, S. et al. Recent Walker circulation strengthening and Pacific cooling amplified by Atlantic warming. *Nat. Clim. Change* **4**, 888–892 (2014).
36. Li, X., Xie, S. P., Gille, S. T. & Yoo, C. Atlantic-induced pan-tropical climate change over the past three decades. *Nat. Clim. Change* **6**, 275–279 (2016).
37. Sun, C. et al. Western tropical Pacific multidecadal variability forced by the Atlantic multidecadal oscillation. *Nat. Commun.* **8**, 15998 (2017).

38. Collins, M. et al. The impact of global warming on the tropical Pacific Ocean and El Niño. *Nat. Geosci.* **3**, 391–397 (2010).

39. Vecchi, G. A. & Soden, B. J. Global warming and the weakening of the tropical circulation. *J. Clim.* **20**, 4316–4340 (2007).

40. Vallis, G. K., Zurita-Gotor, P., Cairns, C. & Kidston, J. Response of the large-scale structure of the atmosphere to global warming. *Q. J. R. Meteorol. Soc.* **141**, 1479–1501 (2015).

41. Raphael, M. N. et al. The Amundsen Sea Low: variability, change, and impact on Antarctic climate. *Bull. Am. Meteorol. Soc.* **97**, 111–121 (2016).

42. Kosaka, Y. & Xie, S. P. Recent global-warming hiatus tied to equatorial Pacific surface cooling. *Nature* **501**, 403–407 (2013).

43. Timmermann, A. et al. El Niño–Southern Oscillation complexity. *Nature* **559**, 535–545 (2018).

44. Ding, Q., Steig, E. J., Battisti, D. S. & Küttel, M. Winter warming in West Antarctica caused by central tropical Pacific warming. *Nat. Geosci.* **4**, 398–403 (2011).

45. Holland, P. R., Bracegirdle, T. J., Dutrieux, P., Jenkins, A. & Steig, E. J. West Antarctic ice loss influenced by internal climate variability and anthropogenic forcing. *Nat. Geosci.* **12**, 718–724 (2019).

46. Lynch-Stieglitz, J. The Atlantic Meridional Overturning Circulation and abrupt climate change. *Ann. Rev. Mar. Sci.* **9**, 83–104 (2016).

47. Monteagudo, M. M., Lynch-Stieglitz, J., Marchitto, T. M. & Schmidt, M. W. Central equatorial Pacific cooling during the Last Glacial Maximum. *Geophys. Res. Lett.* **48**, e2020GL088592 (2021). https://doi.org/10.1029/2020gl088592

48. DiNezio, P. N. et al. The response of the Walker circulation to Last Glacial Maximum forcing: implications for detection in proxies. *Paleoceanography* https://doi.org/10.1029/2010PA002083 (2011).

49. Lund, D. C., Lynch-Stieglitz, J. & Curry, W. B. Gulf Stream density structure and transport during the past millennium. *Nature* **444**, 601–604 (2006).

50. Wanamaker, A. D. et al. Surface changes in the North Atlantic meridional overturning circulation during the last millennium. *Nat. Commun.* **3**, 899 (2012).

51. Sachs, J. P. et al. Southward movement of the Pacific intertropical convergence zone AD 1400–1850. *Nat. Geosci.* **2**, 519–525 (2009).

52. Yan, H. et al. Dynamics of the intertropical convergence zone over the western Pacific during the Little Ice Age. *Nat. Geosci.* **8**, 315–320 (2015).

53. L'Heureux, M. L., Lee, S. & Lyon, B. Recent multidecadal strengthening of the Walker circulation across the tropical Pacific. *Nat. Clim. Change* **3**, 571–576 (2013).

54. Stachnik, J. P. & Schumacher, C. A comparison of the Hadley circulation in modern reanalyses. *J. Geophys. Res. Atmos* **116**, D22102 (2011).

55. Purich, A. et al. Tropical Pacific SST drivers of recent Antarctic sea ice trends. *J. Clim.* **29**, 8931–8948 (2016).

Methods

Global climate model. The global climate model used in this study is the National Centre for Atmospheric Research CESM v.1.2, a fully coupled model comprising atmospheric, oceanic, land and sea ice models. The CESM configuration used here is essentially the Community Climate System Model v.4 (CCSM4)[56]. In particular, the atmospheric component is the Community Atmospheric Model v.4 (CAM4) configured at 1.9° × 2.5° spatial resolution and a hybrid sigma-pressure vertical coordinate with 26 layers in the vertical grid, and the land component is the Community Land Model v.4 (CLM4) that runs on the same grid as the atmospheric model. The ocean model is the Parallel Ocean Program v.2 (POP2), set with a displaced-pole in the Northern Hemisphere over Greenland at 80° N, 40° W. The horizontal grid is nearly uniform in longitude (~1.13°) and variable in latitude (0.27° at the Equator, increasing to 0.65° at 60° N in the western North Pacific), with 60 vertical levels varying in thickness from 10 m near the surface to 250 m at depth. The sea ice component is the Community Ice Code v.4 (CICE4), which runs on the same grid as the ocean model. All model components iterate via a coupling architecture that allows the exchange of freshwater, momentum and heat fluxes between components.

The model used here has been shown to have a good representation of the AMOC in a modern era setting[23]. The model has also been shown to simulate the Pacific mean state and variability relatively accurately compared to other climate models. For example, the model has a reduced cold tongue bias and improved trade wind metrics[24], which are key to controlling the position and strength of the Walker circulation (refer to ref. [24], their Fig. 2c, particularly the indices for the equatorial Pacific zonal SST and wind stress biases). Most climate models exhibit stronger biases in the Pacific, with the Walker circulation typically under-represented in models. The good performance of our model in simulating the Pacific mean state also translates into an improved representation of its variability (that is, a better simulation of ENSO[57] and ENSO diversity[58]). Furthermore, this model reproduces Atlantic–Pacific teleconnections in a more realistic way. This is evident in Extended Data Fig. 1 which shows an analysis[59] of intermodel performance in simulating the Atlantic influence on the Pacific, particularly in relation to the Pacific trade wind response to Atlantic–Pacific SST gradients. This analysis demonstrates the superior skill of the model in simulating this interbasin teleconnection compared to other climate models and also that many other climate models perform poorly in this regard.

Experimental design. First we spin up a pre-industrial control climate for 1,000 yr, and from there we branch off five separate ensemble members of both the control simulation (*AMOC-on*) and a perturbed meltwater run (*AMOC-off*), with each being initialized every 10 yr off the control run. The *AMOC-on* control members effectively comprise overlapping 100-yr continuations of the pre-industrial experiment, while the *AMOC-off* runs are identical, only with a constant surface freshwater forcing of 1 Sv applied over the North Atlantic (50° N to 70° N). This meltwater anomaly represents a strong idealized forcing, as also used in previous studies[60,61], intended to trigger the AMOC to collapse within a few decades, equivalent to melting 1% of Greenland per year. When referring to an AMOC 'collapse' or 'shutdown', this corresponds to a weakening of the AMOC from ~24 Sv to just a few Sv (Fig. 1c), with no surface water convectively overturned to the usual 1,500–2,000 m depth where North Atlantic Deep Water is formed. No flux adjustments are used in either simulation. The equilibrium climate response is derived from the ensemble mean difference between the last 50 yr of the *AMOC-off* case and the equivalent 50 yr from the *AMOC-on* run. All climate properties were also re-analysed over the last 20 and 40 yr of the experiments, which revealed robust results. All results presented here are derived from the ensemble mean of the five *AMOC-off* members relative to the corresponding control ensemble set. Wherever statistical significance tests are shown, each member is used to quantify the inter-member variability on the basis of a Student's *t*-test, in addition to the sample of the corresponding number of years being tested.

Climate metrics. Several climate indices are referred to in the text; the method for calculating these metrics is as follows:

(1) Pacific Walker circulation: following past work, the strength of the Walker circulation is calculated as the surface zonal wind speed averaged in the equatorial Pacific (5° S–5° N, 150° E –150° W), which is a measure of the lower branch of the Walker circulation[35,62].

(2) Northern Hadley cell: the strength of the Hadley cell in the Northern Hemisphere is taken to be the maximum value of the streamfunction (Ψ) at 500 hPa (refs. [63,64]), given by

$$\Psi\left(\phi, p\right) = \frac{2\pi a \cos\left(\phi\right)}{g} \int_0^p \bar{v}\left(\phi, p'\right) \mathrm{d}p'$$

where ϕ is latitude, p is atmospheric pressure, a the Earth's radius, g the gravitational acceleration, v the meridional wind, overbar represents the zonal and annual mean and p' is a dummy pressure variable of integration.

(3) Amundsen Sea Low: the magnitude of the Amundsen Sea Low is defined as the area averaged sea-level pressure offshore of western Antarctica, in the rectangular sector bound by 75° S–60° S, 150° W–80° W.

The changes in these climate metrics in the *AMOC-off* simulations are calculated as the mean change of the ensemble average during the shutdown period (years 50–100), relative to the *AMOC-on* ensemble mean. To make comparisons between the model simulations and observed trends since the start of the satellite era (1979–2021), these same three indices were also calculated using the ERA5 reanalysis[65]. Over the period 1979–2021, there has been an overall intensification of the Pacific Walker circulation (strengthening by 6% decade⁻¹), intensification of the northern Hadley cell (by 0.6% decade⁻¹) and a deepening of the Amundsen Sea Low (by on average 0.5 hPa decade⁻¹).

In addition, we analysed a total of 59 projections from the Coupled Model Intercomparison Project (CMIP; including 28 Phase 5 (CMIP5) and 31 Phase 6 (CMIP6) models), to quantify the projected trends of the Pacific Walker circulation under the Representative Concentration Pathway RCP 8.5 and Shared Socioeconomic Pathways SSP 5–8.5 high-end emissions scenarios, respectively. A 51-yr average is selected to filter out variability due to the Interdecadal Pacific Oscillation. This analysis reveals a median projected weakening of 10% during 2050–2100 relative to 1950–2000 (percentage values are quoted to the nearest %). These results are shown in Extended Data Fig. 7.

Data availability

The ERA5 data used in the study can be downloaded from the Copernicus Climate Change Service (C3S) Climate Date Store (https://cds.climate.copernicus.eu/). The CMIP data analysed can be downloaded from the Earth System Grid Federation portal (https://esgf-node.llnl.gov/). Data generated from the coupled climate model simulations can be downloaded from ref. [66].

Code availability

Python scripts used for the analysis described in this study can be obtained from B.O.P. on request.

References

56. Gent, P. R. et al. The Community Climate System Model version 4. *J. Clim.* **24**, 4973–4991 (2011).
57. Deser, C. et al. ENSO and Pacific decadal variability in the Community Climate System Model version 4. *J. Clim.* **25**, 2622–2651 (2012).
58. Capotondi, A. et al. Understanding ENSO diversity. *Bull. Am. Meteorol. Soc.* **96**, 921–938 (2015).
59. Cai, W. et al. Pantropical climate interactions. *Science* **363**, eaav4236 (2019).
60. Manabe, S. & Stouffer, R. J. Simulation of abrupt climate change induced by freshwater input to the North Atlantic Ocean. *Nature* **378**, 165–167 (1995).
61. Stouffer, R. J. et al. Investigating the causes of the response of the thermohaline circulation to past and future climate changes. *J. Clim.* **19**, 1365–1387 (2006).
62. Luo, J.-J., Sasaki, W. & Masumoto, Y. Indian Ocean warming modulates Pacific climate change. *Proc. Natl Acad. Sci. USA* **109**, 18701–18706 (2012).
63. Chemke, R. & Polvani, L. M. Opposite tropical circulation trends in climate models and in reanalyses. *Nat. Geosci.* **12**, 528–532 (2019).
64. Kang, S. M., Deser, C. & Polvani, L. M. Uncertainty in climate change projections of the Hadley circulation: the role of internal variability. *J. Clim.* **26**, 7541–7554 (2013).
65. Hersbach, H. et al. The ERA5 global reanalysis. *Q. J. R. Meteorol. Soc.* **146**, 1999–2049 (2020).
66. Orihuela-Pinto, B., England, M. H. & Taschetto, A. S. Interbasin and interhemispheric impacts of a collapsed Atlantic Overturning Circulation. Mendeley Data, v.1 (2022); https://doi.org/10.17632/swxxfc45t2.1

Acknowledgements

Author contributions

M.H.E. conceived the design and scope of the study. B.O.P. undertook the model simulations, data analysis and plotted the figures with input from M.H.E. and A.S.T. A.S.T. produced the schematic diagram with input from M.H.E. and B.O.P. All authors contributed to the analysis, discussion, interpretation and writing of the paper.

Competing interests

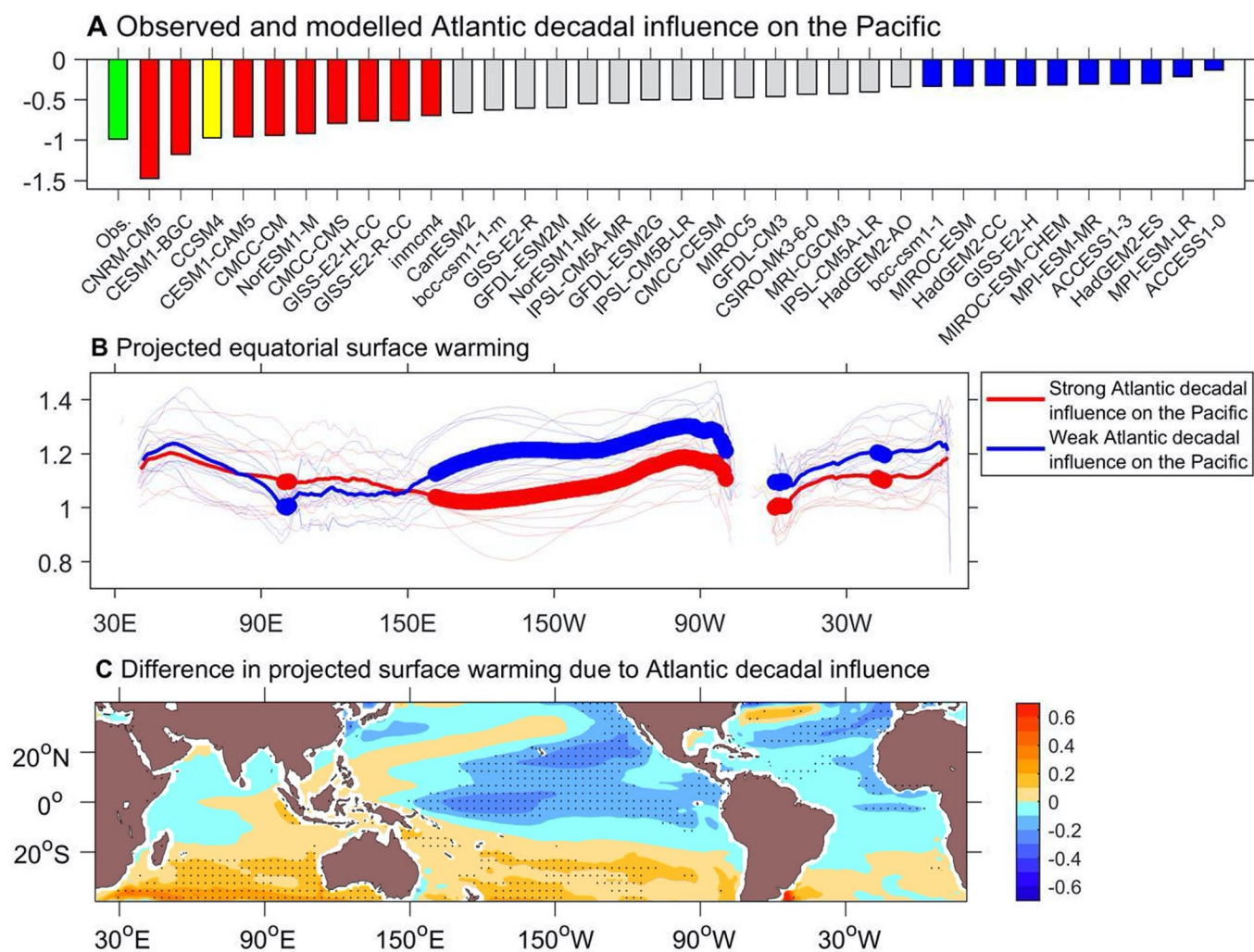The authors declare no competing interests.

Additional information

A Observed and modelled Atlantic decadal influence on the Pacific

B Projected equatorial surface warming

Strong Atlantic decadal influence on the Pacific
Weak Atlantic decadal influence on the Pacific

C Difference in projected surface warming due to Atlantic decadal influence

Extended Data Fig. 1 | Model intercomparison of Atlantic–Pacific teleconnection strength. (**a**) Regressions between 11-year running trends in Pacific trade winds and 11-year running trends in the Atlantic–Pacific trans-basin index. Shown in red and blue are the models that are the most and least similar in reproducing the observed regressions (green bar), respectively, with the yellow bar indicating CESM1-CAM4 (equivalent to CCSM4) as used in this study. The Atlantic–Pacific trans-basin index is defined as the tropical Atlantic (20°S to 20°N; 70°W to 20°E) minus tropical Pacific (20°S to 20°N; 121°E to 90°W) SST gradient. (**b**) Future projections of equatorial (5°S to 5°N) SST (per degree of global warming) in two ensembles of 10 CMIP5 models (thin curves) with a strong (red) and weak (blue) coupling between decadal trends of the Atlantic–Pacific trans-basin index and equatorial Pacific trade winds. Changes are calculated as the difference in averages between RCP8.5 2070–2099 and the historical 1980–2009 period, divided by the global mean SST change over the same periods. The broad thick curves indicate where the difference between the two ensemble means (indicated by solid curves) is significant at 95% confidence level, based on a Student t-test. (**c**) Difference in climatological SST changes between the two 10-model ensemble means. Stippling indicates areas where the ensemble mean difference is significant at the 95% confidence level, based on a Student t-test. The colour scale in (c) indicates temperature in °C. Figure is an extended version of Fig. 5 from ref. [59].
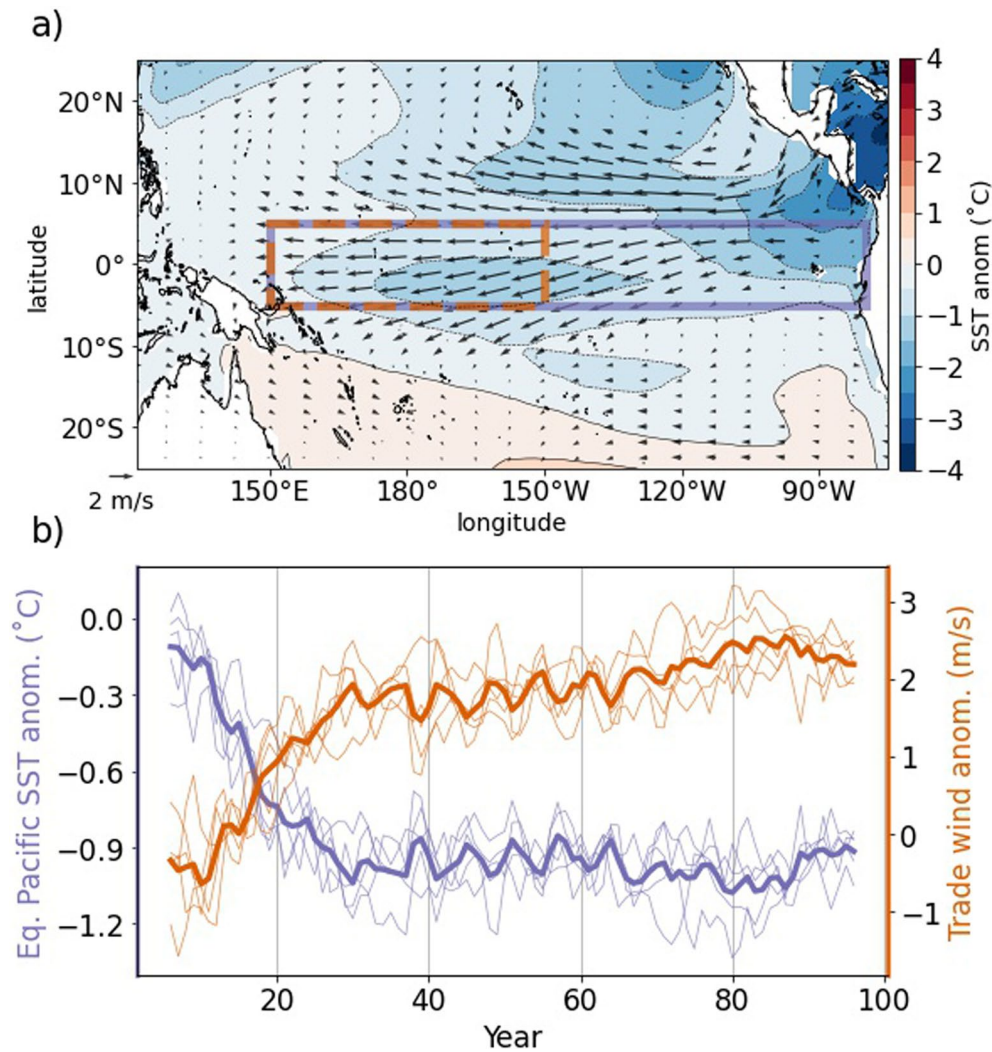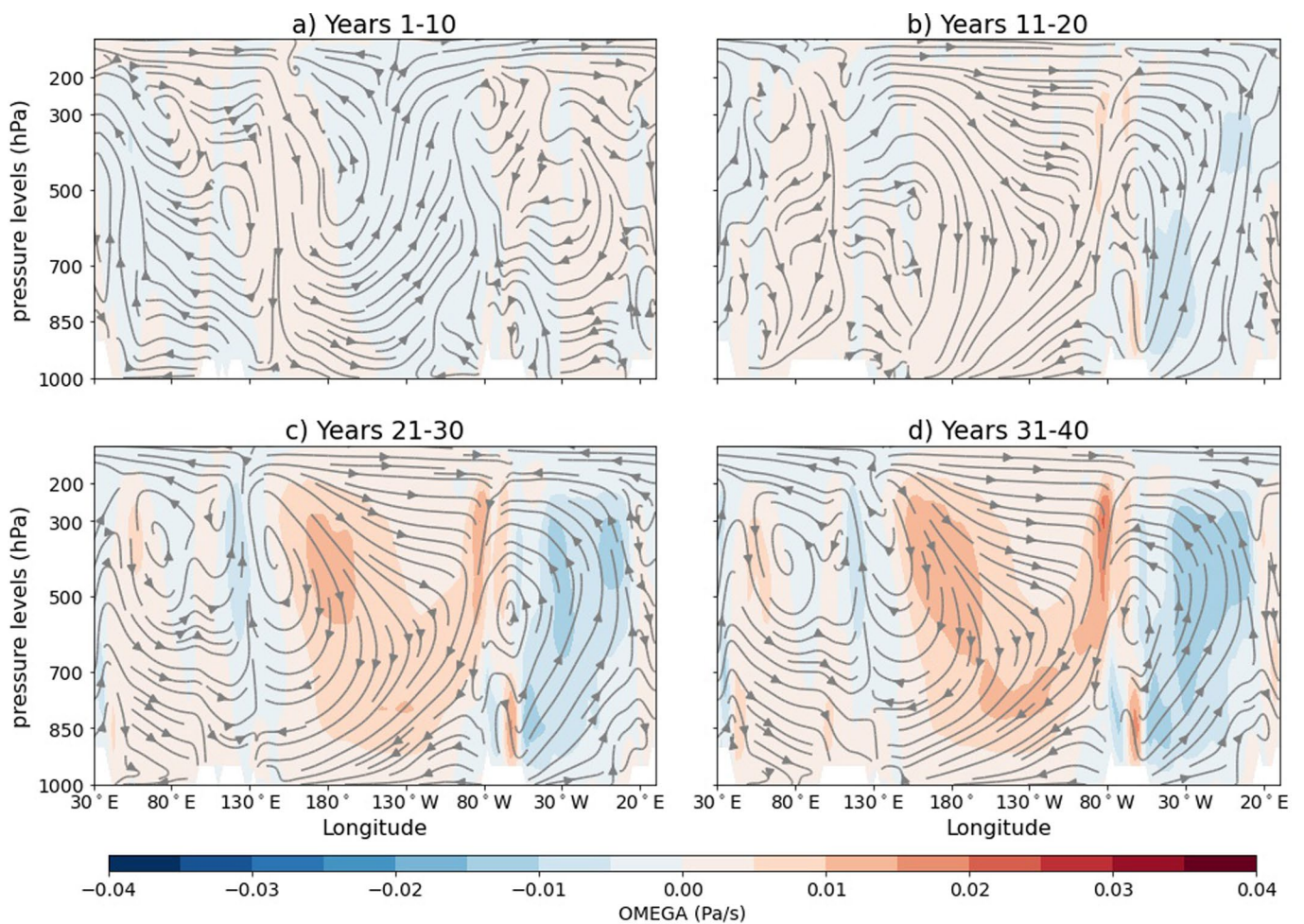
Extended Data Fig. 2 | Transient evolution of the Pacific climate response to AMOC shutdown. (**a**) Anomalies of sea surface temperature (°C) and 850 hPa winds (m/s; overlaid as vectors), calculated for *AMOC-off* relative to *AMOC-on* and averaged over years 51–100 of the ensemble sets of experiments. (**b**) Transient evolution of the difference between *AMOC-off* and *AMOC-on* for equatorial Pacific sea surface temperature (°C; purple line) and Pacific trade winds, calculated based on the 850 hPa zonal wind speed (m/s; orange line); the latter is a measure of the strength of the lower branch of the Walker circulation[35,62]. Time series shown are 10 year running means. The 5 ensemble member difference time series are shown for each ensemble in thin lines, with the ensemble averages shown in solid bold lines. The areas for the spatial averages of each variable are shown in panel (a) as colour-coded rectangles.
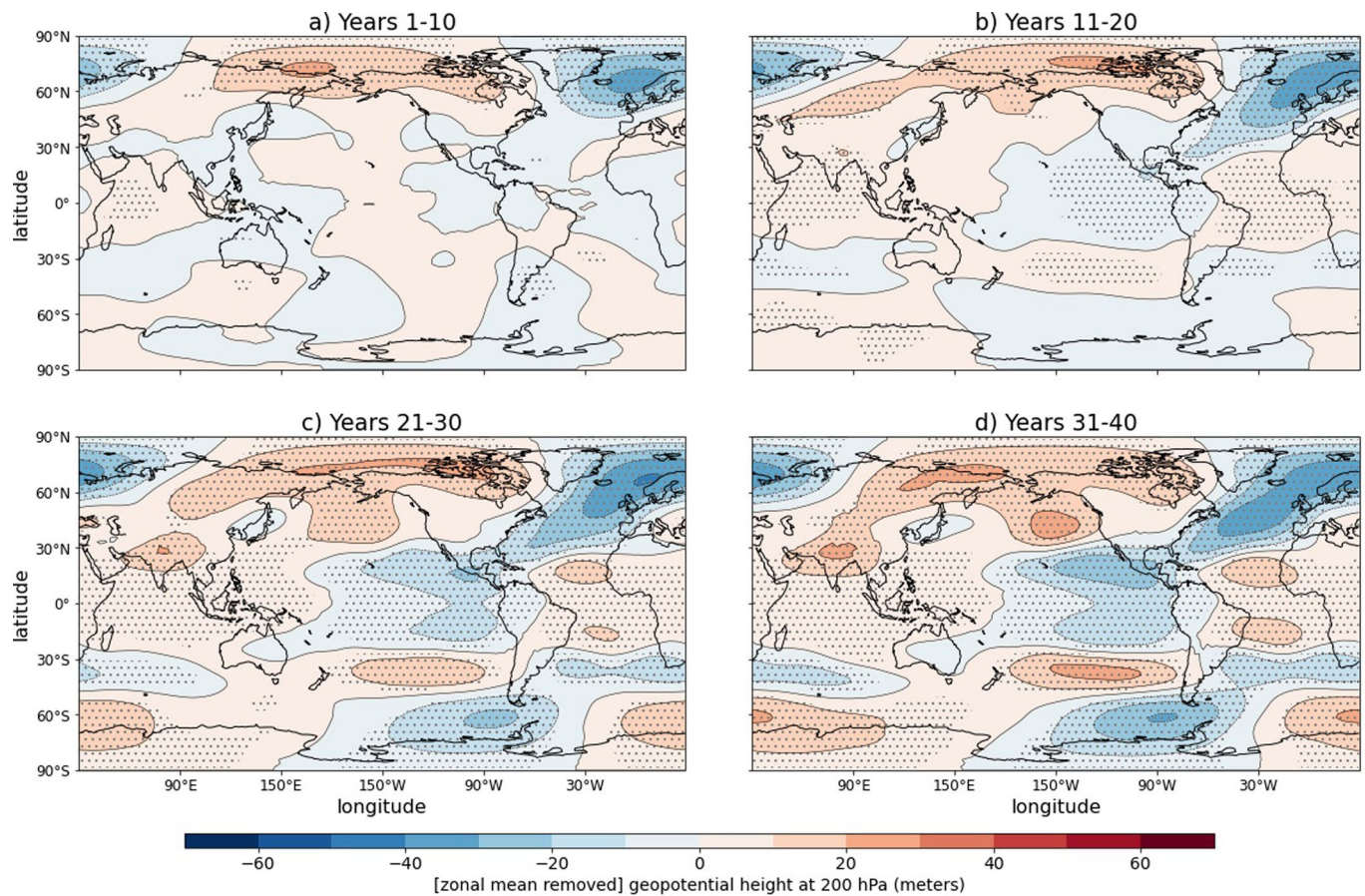
Extended Data Fig. 3 | Transient evolution of geopotential height at 200 hPa in response to AMOC shutdown. Anomalies of geopotential height at 200 hPa with zonal mean removed in response to a meltwater-induced AMOC shutdown (*AMOC-off* ensemble mean minus *AMOC-on* ensemble mean). Each panel shows decadal mean anomalies of geopotential height at 200 hPa with zonal mean removed (m), with regions showing significant differences hatched based on a Student *t-test* at 95% significance level.
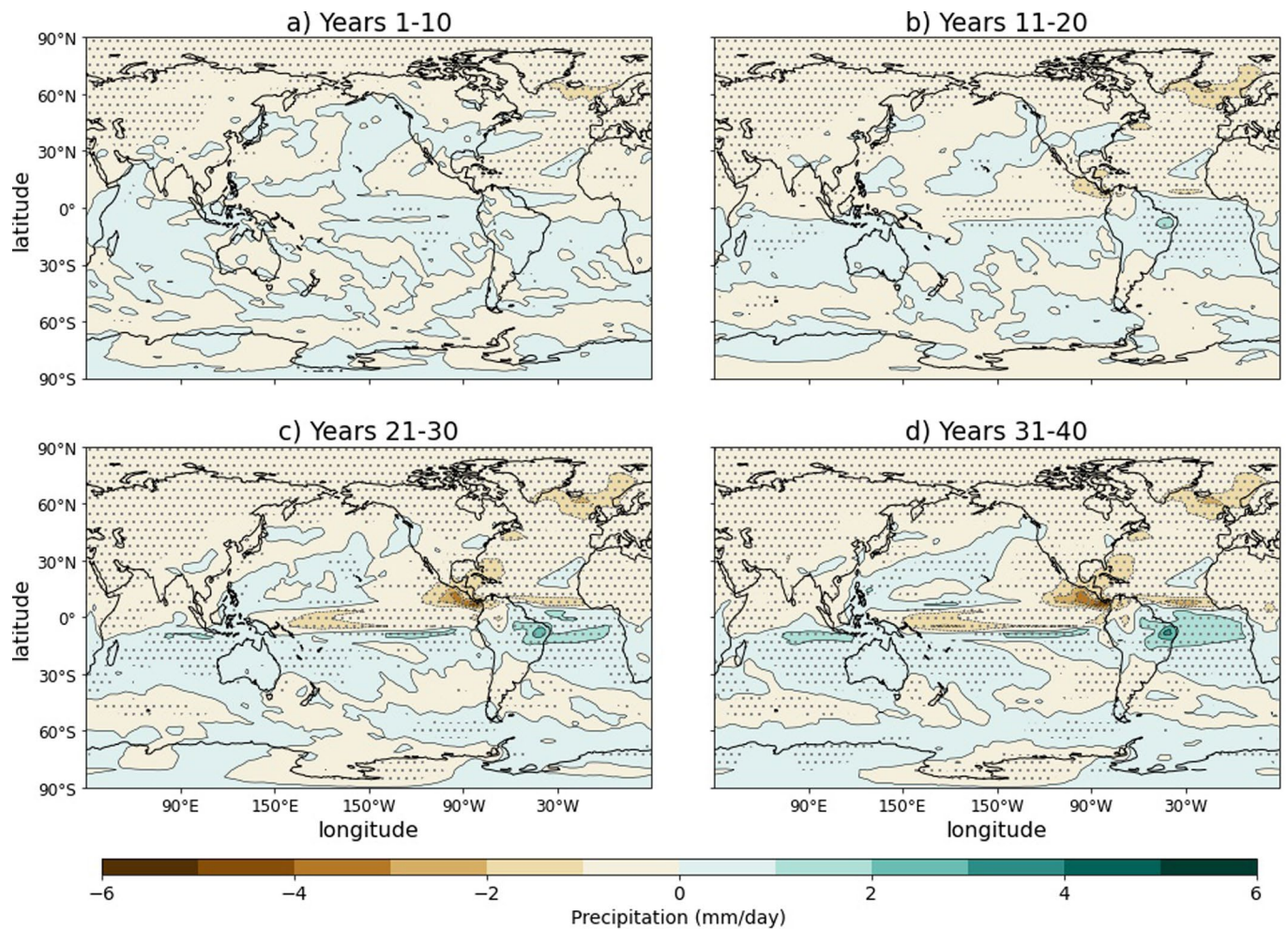
Extended Data Fig. 4 | Transient evolution of precipitation in response to AMOC shutdown. Anomalies are shown as the *AMOC-off* ensemble mean minus *AMOC-on* ensemble mean. Each panel shows decadal mean anomalies of precipitation (mm/day), with regions showing significant differences hatched based on a Student t-test at 95% significance level.

Extended Data Fig. 5 | Transient evolution of equatorial atmospheric circulation and vertical velocity in response to AMOC shutdown. Anomalies are shown as the *AMOC-off* ensemble mean minus *AMOC-on* ensemble mean. Each panel shows decadal mean anomalies of equatorial (5°S–5°N) mean atmospheric circulation (streamlines) and vertical velocity (shading; Omega, Pa/s).
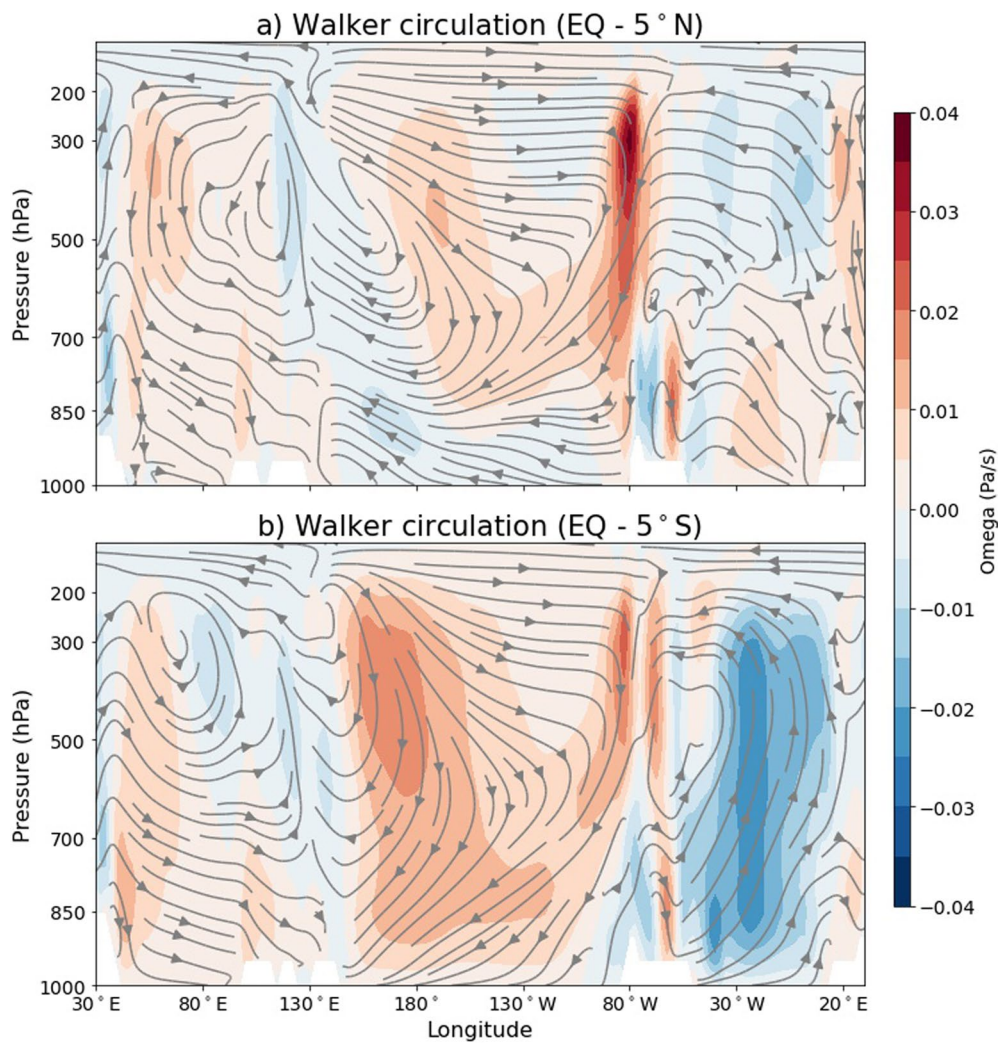
Extended Data Fig. 6 | Decomposition of the Walker circulation response to AMOC shutdown north and south of the Equator. Annual mean anomalies of equatorial mean atmospheric circulation (streamlines) and vertical velocity (shading; Omega, Pa/s) in response to an AMOC shutdown (*AMOC-off* ensemble mean minus *AMOC-on* ensemble mean, averaged over years 51–100) decomposed into the latitudes (**a**) north (0°-5°N) and (**b**) south (5°S-0°) of the Equator.
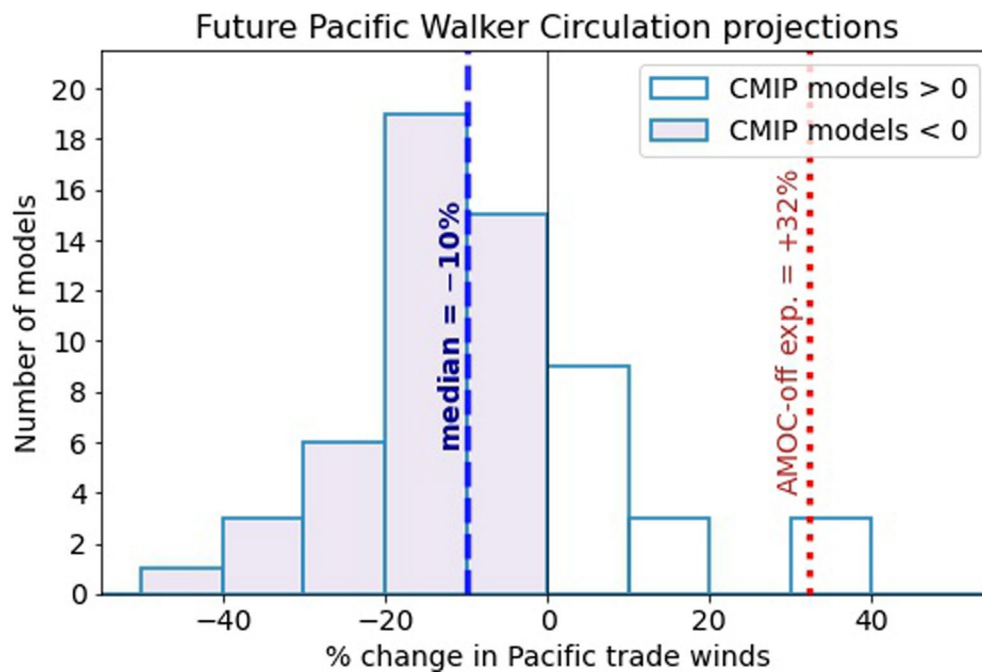
Extended Data Fig. 7 | Comparison between the Walker circulation increase due to AMOC shutdown vs. that projected by climate models for 2050–2100. Histogram of future projections in the lower branch of the Pacific Walker circulation, as measured by the percentage change in 850 hPa zonal winds averaged over the equatorial Pacific (5°S–5°N, 150°E –150°W)[35,62] during the 2050–2100 period relative to 1950–2000 (blue dashed line indicates the median change). A 51-year average is selected to filter out variability due to the Interdecadal Pacific Oscillation. All up 28 CMIP5 and 31 CMIP6 models are used under the RCP8.5 and SSP5-8.5 high-end emission scenarios, respectively. The red dotted line indicates the change of the same metric in the *AMOC-off* ensemble mean, relative to *AMOC-on*. Percentage values (%) quoted are rounded to the nearest percentage point.